Ageing Studies of Mega Battery Packs for Grid Storage Applications Using Physics Based Modeling

K. S. N. Vikrant
Department of Materials Science & Engr.
Indian Institute of Technology Delhi
New Delhi, India
ksnvikrant@iitd.ac.in

Tom G. Tranter
Ionworks Technologies Inc
5831 Forward Ave #1276
Pittsburgh, USA
t.g.tranter@gmail.com

Gavin M. Wiggins
Computing & Computational Sci. Directorate
Oak Ridge National Laboratory
Oak Ridge, TN 37831, USA
wigginsg@ornl.gov

Dan J. L. Brett
Electrochemical Innovation Lab
University College
London, UK
d.brett@ucl.ac.uk

Srikanth Allu
Computing & Computational Sci. Directorate
Oak Ridge National Laboratory
Oak Ridge,TN 37831, USA
allus@ornl.gov

***Abstract*—The lower Levelized Cost of Electricity (LCOE) from wind and solar photovoltaics has enabled for greater integration of variable energy resources with energy storage technologies such as larger centralized lithium-ion battery megapacks (with 1MWh total energy and 500V rating) to provide utility-scale services to grid operators. The daily cycling of standalone lithium-ion grid storage will reduce the battery cells' capacity due to several degradation mechanisms. A comprehensive physics-based Python^{tm} framework called Liionpack was developed to estimate these megapacks' remaining life and ageing. The study includes various degradation mechanisms coupled to the electrochemical-thermal model at the pack level. The effect of the inhomogeneities from cell-to-cell thermodynamic and kinetic properties for different working conditions including temperature and charge/discharge protocols on the ageing of a megapack are presented here.**

***Index Terms*—Physical degradation mechanisms; Cell ageing; Battery pack ageing; PyBaMM; liionpack.**

I. Introduction

The excess or unused (curtailed) energy can be stored in grid-level energy storage systems during peak generation periods and used when required [1]–[3]. Lithium-ion battery packs are one of the promising grid-level storage systems due to their high energy density, cycle life, lighter weights, and low self-discharge [4], [5]. Also, lithium-ion battery packs are operable at grid-level for long and short duration storage for both frequent and infrequent discharge conditions [6]. The battery's useful life and period of optimum performance are critical to application design as well as environmental impact [7], [8]. Understanding the ageing and degradation mechanisms of the battery cell under various operating conditions can prevent premature failure, avoid safety issue, and increase opportunities for secondary use. Cycling and even the resting state of lithium-ion batteries result in degradation of their capacity [7]–[9]. One of the primary reasons for the ageing of batteries originates from the degradation of electrochemical and chemomechanical physical processes of the cell during cycling. Many ageing mechanisms and associated modeling techniques have been identified for lithium-ion batteries of which Reniers et.al., provide a good overview [10]. The major mechanisms of concern include growth of the solid electrolyte interphase (SEI) layer, surface cracking of the electrode, loss of active electrode material, electrolyte oxidation at the positive electrode, and lithium plating [7], [8].

Growth of the SEI layer on negative electrode is a major cause of lithium-ion battery ageing due to loss of lithium inventory. However, the growth of the initial layer does inhibit further electrolyte decomposition and negative electrode degradation. The SEI is a complex structure but is often considered to have a bilayer composition, with the dense inner layer containing inorganic salts, and a soft outer layer based on the organic reaction products. The growth of SEI is often modeled with a Tafel equation [10]–[13]. The intercalation and de-intercalation of ions cause expansion and contraction of electrode materials, resulting in mechanical stresses which in turn cause material fatigue as well as crack formation and propagation. The cracks create new solid-electrolyte interfaces and allow more SEI growth on the fresh surfaces, leading to more loss of cyclable lithium at the negative electrode [10], [13]. Lithium plating is a faradaic reaction in which Li+ ions in the electrolyte form lithium metal on the surface of the negative electrode, instead of intercalating. This mainly

This work is supported by the DOE Office of Electricity Dr, Imre Gyuk and was carried out at Oak Ridge National Laboratory under Contract No. DE-AC05-00OR22725 with UT-Battelle, LLC. This manuscript has been authored by UT-Battelle, LLC, under contract DE-AC05-00OR22725 with the US Department of Energy (DOE). The US government retains and the publisher, by accepting the article for publication, acknowledges that the US government retains a nonexclusive, paid-up, irrevocable, worldwide license to publish or reproduce the published form of this manuscript, or allow others to do so, for US government purposes. DOE will provide public access to these results of federally sponsored research in accordance with the DOE Public Access Plan (http://energy.gov/downloads/doe-public-access-plan). Also, the authors acknowledge the funding and support of the Faraday Institution's multi-scale modelling project and Innovate UK.

happens during fast charging when the electrostatic potential of the negative electrode is less than that of a Li/Li+ reference electrode, such as plating overpotential [14] and is exacerbated at lower operating temperatures.

In addition to modeling an individual battery cell, several authors have contributed to understanding the impact of cell-to-cell variability on overall battery pack performance. These studies include both experimental and simulation avenues. Numerous experimental studies show that cell-to-cell variability exists, including differences in electrode thickness, porosity, initial state-of-charge (SOC), etc. [15], [16]. Even the physico-chemical properties can be different for each cell. In addition to internal parameters of the cell, external parameters such as connections to busbars can also contribute to the variability. Numerical simulations studies have been conducted on different cell chemistries, such as LFP, NMC, LMO, [17]–[19] and have tried to predict the change in capacity, resistance, SOC, state-of-health (SOH) [20]. However, none of these analyses consider studies on the battery pack ageing due to side reactions and loss of active material during cyclic operation.

The paper emphasizes pack degradation and does not present single-cell degradation modeling, which several authors have already published for NMC and graphite chemistry [10], [21], [22]. This work focuses on the lithium-ion battery pack modeling approach to estimate ageing and degradation effects from various operating conditions. The pack level modeling techniques are discussed, and results from the simulations are presented. The megapack setup is used to understand the degradation associated with individual cells and the change in cell-to-cell output response from the variability related to initial conditions, busbars, internal connecting resistors, and terminal connections. Also, a study on pack ageing due to the distribution of initial SOC was presented from the potential use of secondary usage of battery cells in a pack for grid storage application. Specifically, we considered a constant charge and discharge current profile in this study. In the future, we will develop the framework for variable current/voltage/load profiling of a grid megapack. Finally, conclusions based on the megapack simulation results are presented along with the future steps for pack modeling.

II. METHODS

In this section the lithium-ion cell and battery pack models are discussed. The cell is simulated using a single particle model (SPM) while the pack model consists of a network of cell models connected via an electrical circuit of terminals and resistors. The ageing and degradation mechanisms utilized in the models are also mentioned.

A. Single Particle Model

The Single Particle Model (SPM) is a representative electrochemical model of the lithium-ion cell considering a sphere for each electrode [10], [23]–[26]. The model accounts for diffusion in both negative and positive electrodes referred as $i \in \{-,+\}$ and assumes uniform kinetics. The time (t) evolution of lithium concentration c_i, in the spherical particle of electrodes having radius r is given as [23]–[26]:

$$\frac{\partial c_i(r,t)}{\partial t} = \frac{D_i}{r^2}\frac{\partial}{\partial r}\Big(r^2\frac{\partial c_i(r,t)}{\partial r}\Big) \tag{1}$$

where D_i is solid state diffusivity of lithium in spherical particle of negative/positive electrode. A zero-flux boundary condition is imposed at the center of the particle via $D_i\frac{\partial c_i(r,t)}{\partial r}\Big|_{r=0} = 0$ and the outer surface is subjected to an intercalation flux j_i having the boundary as $D_i\frac{\partial c_i(r,t)}{\partial r}\Big|_{r=R_i} = -j_i$. The total flux is $j_T = j_i + j_{sei} + j_{pl} = \frac{I}{V_i a_i n F}$ which is the sum of intercalation flux along with fluxes due to side reactions such as SEI growth and plating kinetics. The volume fraction of active material ϵ_i and surface area a_i is correlated as $a_i = 3\frac{\epsilon_i}{R_i}$. The fluxes associated to side reactions due to SEI growth and plating growth are given by j_{sei} and j_{pl}, respectively. I is the total applied current, V_i is electrode volume, n is number of electrons, and F is Faraday's constant.

The reaction limited SEI growth flux,j_{sei} is given by [11]–[13]:

$$\begin{aligned} j_{sei} &= -\frac{i_{sei}}{nF} = -\frac{i_{\circ,sei}}{nF}\exp(-\frac{\alpha_{sei}nF\eta_{sei}}{RT}) \\ \frac{\partial \delta_{sei}}{\partial t} &= \frac{i_{sei}M_{sei}}{\rho nF} \\ \eta_{sei} &= \eta_i + \phi_{OCV} - \phi_{\circ,sei} + \rho_{sei}\delta_{sei}I \end{aligned} \tag{2}$$

where $i_{\circ,sei}$ is the exchange current density for SEI reaction, α_{sei} is SEI charge transfer coefficient, M_{sei} is molecular weight of SEI layer, ρ_{sei} is density of SEI layer, η_{sei} is SEI overpotential, η_i is intercalation overpotential, ϕ_{OCV} is equilibrium potential of negative electrode, $\phi_{\circ,sei}$ is SEI equilibrium potential.

The lithium plating and stripping flux, j_{pl} is given by [27], [28]:

$$\begin{aligned} j_{pl} &= -\frac{i_{pl}}{nF} = -\frac{i_{\circ,pl}}{nF}\Big(\exp(\frac{(1-\alpha_{pl})nF\eta_{pl}}{RT}) \\ &- \exp(\frac{-\alpha_{pl}nF\eta_{pl}}{RT})\Big) \\ \frac{\partial \delta_{pl}}{\partial t} &= \frac{i_{pl}M_{pl}}{\rho_{pl}nF} \\ \eta_{pl} &= \eta_i + \phi_{OCV} + \rho_{sei}\delta_{sei}I \end{aligned} \tag{3}$$

where, $i_{\circ,pl}$ is the exchange current density for plating reaction, α_{pl} is plating charge transfer coefficient, M_{pl} is molecular weight of metallic lithium layer, ρ_{pl} is density of metallic lithium, η_{pl} is the plating overpotential.

The stress driven loss of active material (LAM) is given by [29]–[31] $\frac{\partial \epsilon_i}{\partial t} = \beta\Big(\frac{\Delta\sigma_h}{\sigma_y}\Big)^m$ where σ_h is hydrostatic stress, σ_y is yield strength, and β, m are LAM parameters. The other possible degradation mechanisms which are not considered in the model are crack growth, pore-clogging, and electrolyte oxidation at the positive electrode [7]–[9], [32]. In this study, we utilize a single-cell parameter set collected by Chen and coauthors [22] for the LG M50T cylindrical commercial cell,

which comprises an NMC positive electrode and 90%graphite-10%SiO_x negative electrode. The electrochemical parameters of the Chen et.al., chemistry is already implemented in the PyBaMM framework for a single cell. In addition to these parameters, the mechanical parameters for LAM degradation are listed in Table 1 of the Supplementary Information. The SPM degradation mechanisms, and lumped thermal models for single cells are implemented and validated with the experimental data using the open-source PyBaMM Python package [21].

B. Battery Pack Model

The open-source Python package named Liionpack [33] is a battery pack simulation tool that uses the PyBAMM framework. In this work, Liionpack is used to analyze battery pack capacity degradation under SEI growth, irreversible lithium plating, as well as stress-driven loss of active material for the following cases: (1) variability due to busbar and connector resistances, (2) variability due to terminal connections and (3) variability due to initial SOC of cells. The typical battery pack equivalent circuit is shown in Supplementary Figure 2. The battery pack model consists of 50,000 cells in a 400p125s configuration to represent a megapack of ∼1MWh energy and 500V rating.For a 400p125s battery pack model, p is the number of cells in parallel and s is the number of cells in series.

The constant current cycling protocol was used to study the ageing of the battery pack. First, the pack is charged at 500 A for 10 minutes, then rested for 10 minutes, followed by discharge at 500 A for 10 minutes, and rested for 10 minutes. The nominal capacity of a single cell in the megapack is 5 Ah. The test protocol is a case study of a short duration storage system with a frequent discharge, emphasizing an accelerated test to quantify the effect of degradation modes on battery pack ageing. Currently, the framework is limited to handling a constant battery pack current protocol; however, in future work, voltage and power profiles will be implemented. The initial temperature of the battery pack is set to 25°C. The megapack simulations are carried out on the VIBE JupyterHub [34] where each simulation used 128 CPU cores with access to ∼500 GB of memory. The wall time of each simulation for 500 equivalent cycles is ∼38 hours.

III. RESULTS & DISCUSSION

Figure 1 (a) shows the pack terminal voltage of the 400p125s configuration subjected to constant current protocol as described in the Methods section. In this analysis, all the cells are identical by having the same macroscopic/microscopic properties connected with negligible busbar/connector resistances. The SEI growth, lithium plating, and LAM ageing modes are considered in the analysis. The pack terminal voltage is slightly decreased at the end of the cyclic operation owing to the degradation mechanisms of SEI and lithium plating kinetics which result in a loss of lithium inventory. Figure 1 (b) shows the non-linear percentage increase of change in the internal resistance of the pack with the number of cycles due to increasing cell resistances in the pack. The increase in overall pack resistance is mainly because of the increase in SEI layer thickness in individual cells. The percentage change in the internal resistance of the battery pack is obtained as $\frac{R_{pack,cycle}-R_{pack,\circ}}{R_{pack,\circ}} * 100$, where $R_{pack,cycle}$ is pack resistance at a specific cycle, and $R_{pack,\circ}$ is initial pack resistance. The pack resistance at any given cycle is $R_{pack,cycle} = \frac{1}{\left(\sum_{j=1}^{p} \frac{1}{\left(\sum_{i=1}^{s} R_i\right)}\right)}$, where p, number of cells in parallel, s, number of cells in series, R_i is the internal resistance of the i-th cell. Figure 1 (c) shows the capacity fade of the battery pack. The degradation of cells from SEI and plating kinetics are due to the loss of lithium inventory which results in a decrease in battery pack capacity and also decreases the 'overall stored energy' during the cyclic operation (see inset (d)). Here, the capacity of the battery pack is obtained as $Q_{pack} = min\left(\sum_{i=1}^{p} Q_i\right)_{Ns}$, where Q_i is the capacity of the i-th cell, and the energy of the pack is $E_{pack} = Q_{pack}V_{pack}$. Figure 1 (e) shows the power fade of the battery pack $P_{pack} = \frac{V_{pack}^2}{R_{pack}}$ results in a decrease in pack voltage and an increase in the internal resistance due to degradation mechanisms.

In Figure 2, we show the effect of initial SOC distribution on the individual capacity loss of cells in a megapack. The initial SOC of cells having a Gaussian distribution with a mean SOC value=0.5 and a standard deviation of 0.1 is randomly distributed in the 400p125s megapack configuration (see Figure 2 (a)). Figure 2 (b) shows a capacity loss of individual cells based on the initial SOC distribution with negligible busbar and connector resistance. More significant ageing occurs in the cells with larger SOC because of an increase in degradation from SEI growth and plating with large negative interfacial potentials for side reactions. Also, the loss of active material due to stress-induced effects during intercalation and de-intercalation is high for large SOC in a cycling protocol for the given chemistry. Consequently, a distribution of capacity losses of cells in the battery pack are observed based on the initial distribution of SOC. Figure 2 (c) shows an additional effect from busbar and connector resistances having a left end terminal. The calculations emphasize that cells to the left side undergo additional capacity loss due to circuit connectors.

Balancing of currents in the megapack after 500 cycles are shown statistically in Figure 3 during the rest period. In the presence of busbar and connector resistors, the megapack balances statistically by having small negative and positive currents in each group of cells while the total battery pack current is zero (black dashed lines). The positive and negative currents are a result of current flowing in the busbar during the rest period resulting in balancing of the currents as shown in Figure 3 (a) and (b). The balanced currents are negligible in the absence of busbar/internal connectors resistance case as shown in Figure 3 (c) and (d). The initial SOC Gaussian distribution in the cells of a battery pack exhibits a different voltage response in the rest period, as shown in Figure 3 (f)

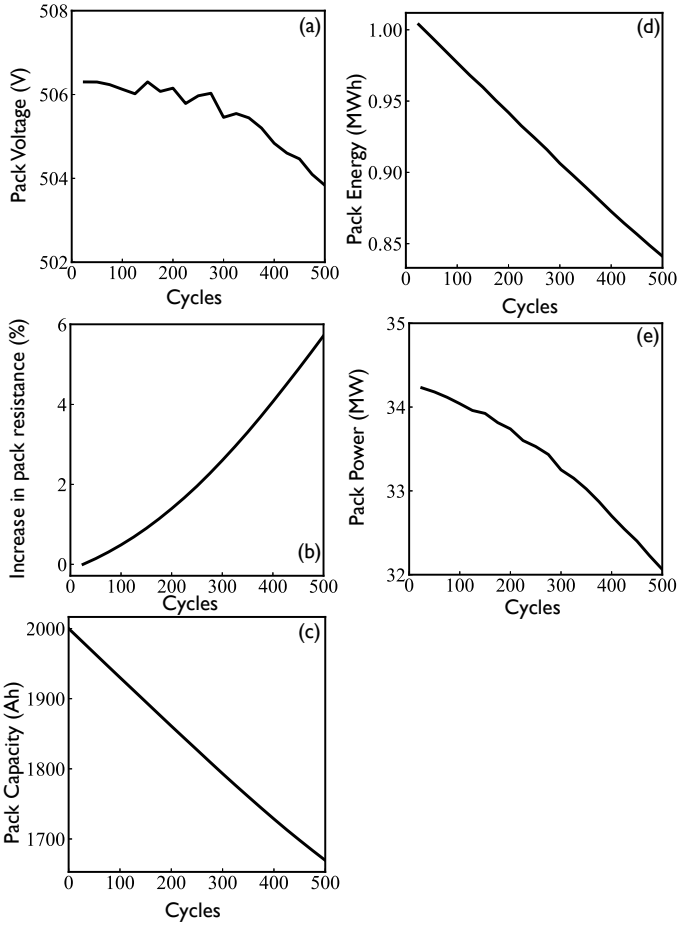

Fig. 1. Terminal voltage (a), percentage increase in internal resistance (b), total capacity (c), total energy (d), and pack power (e) of the battery pack as a function of equivalent cycles for a 400p125s configuration with negligible connector and busbar resistances.

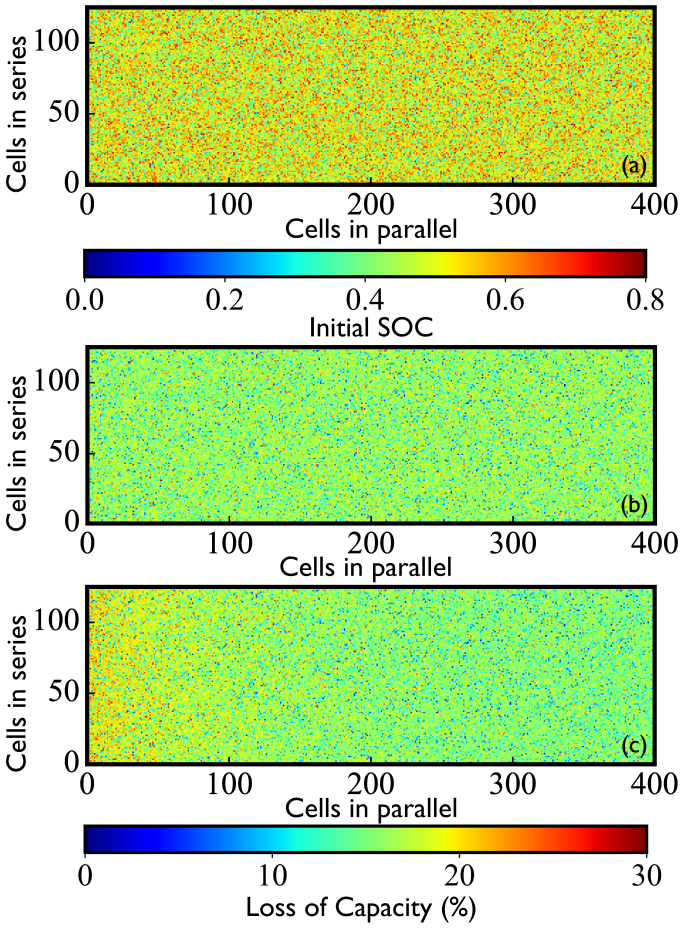

Fig. 2. (Top) A Gaussian distribution of mean SOC=0.5 with standard deviation=0.1 is randomly distributed for a megapack of 400p125s configuration. Capacity loss of cells in a megapack of 400p125s configuration after 500 cycles having a negligible busbar and connector resistance (Middle), and with comparable busbar and connector resistance to the internal resistance of cells (Bottom). Both the scenarios have a left-end terminal connection.

compared to same initial SOC which do not change much in voltage response (see Figure 3 (e)).

Figure 4 shows the capacity loss distribution of the megapack subjected to different equivalent ageing cycles. The ageing of the megapack with identical cells connected to the left or right end of the terminal shows that the statistical deviation in loss of capacity increases with an increase in the number of cycles from 100 to 500 (see Figure 4 (a)). Figure 4 (e) shows the corresponding battery pack loss of capacity (solid line) with number cycles, which closely follows the individual minimum cell degradation of the pack (black dotted line), as the number of cells in this category is high. The maximum degradation of a cell is observed at the left terminal (black dashed line). Similarly, in a left-end and right-end terminal connected battery pack, the deviation in loss of capacity is small with the increase in ageing cycles (see Figure 4 (b)). Also, the ageing difference between the maximum degraded cell and the minimum degraded cell is small and battery pack ageing is almost the same as the minimum degradation of cells in a pack (see Figure 4 (f)). Figure 4 (c) shows the capacity loss distribution of the megapack for different cycles for distributed SOC with negligible busbar and connector resistance. Here, the standard deviation of capacity loss in cells has been increased with the number of cycles, indicating that the degradation data of cells in the megapack changes from clustering to a spread-out population. A set of the cell population, the extent of which statistically stands out from the battery pack loss of capacity (colored dashed lines), fails earlier in the battery pack life. The minimum loss of capacity of a cell having a small SOC is observed to follow a linear ageing profile (black dotted line in Figure 4 (g)). However, cells with a large SOC show maximum degradation due to an increase in the rate of side reactions; this results in a non-linear ageing profile (black dashed line). Furthermore, the addition of busbar and connector resistors increases the population of significantly degraded cells (see Figure 4 (d)), and the maximum degradation is observed in cells with large SOC connected to a terminal end. The maximum loss of capacity of a cell in the pack increases from the previous

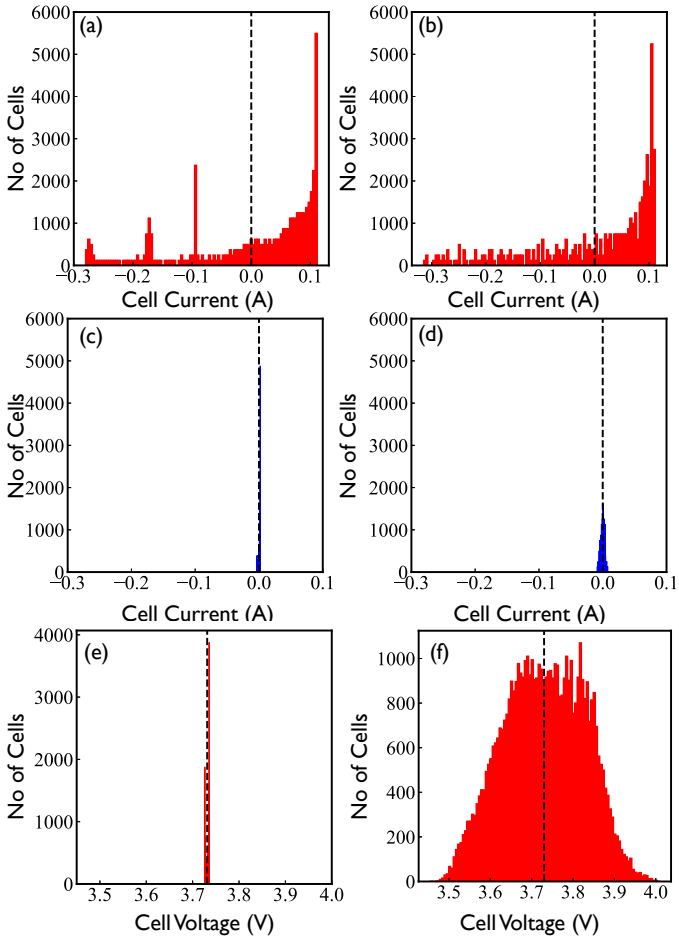

Fig. 3. Current balancing of the megapack in rest period after 500 cycles with identical cells (inset (a), (c)) and distributed SOC(inset (b), inset (d)). Top row (inset (a), (b)) considered busbar and connecting resistors, and middle row (inset (c), (d)) have a negligible busbar and connecting resistors. The corresponding Voltage distribution of the megapack in rest period after 500 cycles with identical cells (inset (e)) and distributed SOC (inset (f)) including busbar and connecting resistors.

case (negligible busbar/connector resistance) due to additional degradation from circuit resistance and terminal connection (black dashed line in Figure 4 (h)). Overall, the pack-level capacity with distributed SOC will age quickly due to the uneven distribution of voltage, resulting in a change in capacity loss and contributing to the ageing of the pack.

IV. CONCLUSIONS

The Liionpack physics-based framework for battery pack lifetime calculations has been used to estimate the remaining life and ageing of a megapack for large scale grid storage applications. The study includes the NMC single-cell data incorporating the physics-based electrochemical-thermal model coupled with various degradation mechanisms. In addition to degradation at the cell level, inhomogeneities from cell-to-cell variability due to deviations of the cell parameters and cell connectors such as busbars, internal resistors, and terminal connections impact the ageing of the battery pack. The ageing

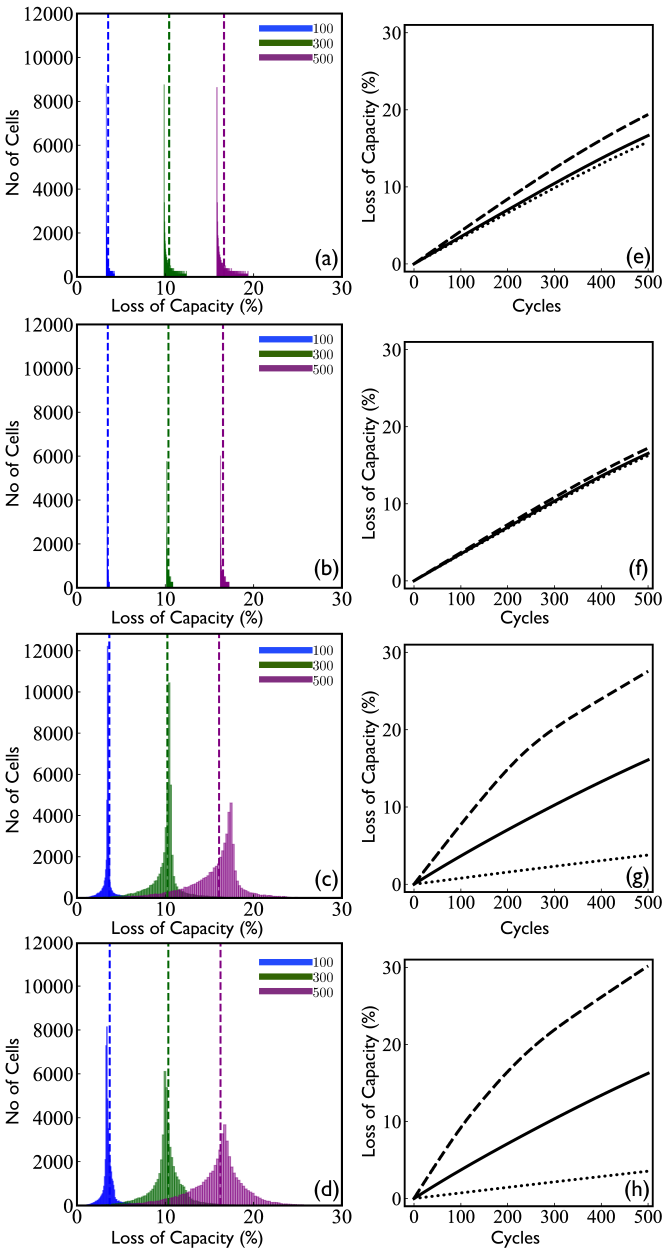

Fig. 4. Capacity loss distribution of the megapack after 100 (blue), 300 (dark green), and 500 (purple) cycles for (a) identical cells with left-end or right-end terminal connection, (b) identical cells with left-end and right-end terminal connections, (c) SOC Gaussian distribution with negligible busbar and connector resistance, (d) SOC Gaussian distribution with busbar and connector resistance. The blue dashed, green dashed and purple dashed lines are battery pack loss of capacity at 100, 300, 500 cycles, respectively. The corresponding loss of battery pack capacity (black solid line), maximum (black dashed line) and minimum (black dotted line) degradation of cells in a pack as a function of ageing cycles are shown from (e)-(h) in the second column for the respective cases.

analysis of the megapack emphasizes that the capacity losses are significant for a cell with high SOC located near the terminal end of the battery pack and highlights that the initial state of cells plays a vital role in the degradation process along with the busbar and terminal connections. In future, we will integrate a battery management system (BMS) in the current framework for active balancing and thermal management of cells of a megapack. While it is beyond the scope of this article, the presented work sets the stage for comprehending the strategies for secondary use of lithium-ion cells in grid-connected energy storage and long-range electrical vehicles.

REFERENCES

[1] H. Chen, T. N. Cong, W. Yang, C. Tan, Y. Li, and Y. Ding, "Progress in electrical energy storage system: A critical review," *Progress in natural science*, vol. 19, no. 3, pp. 291–312, 2009.

[2] C. Lu, H. Xu, X. Pan, and J. Song, "Optimal sizing and control of battery energy storage system for peak load shaving," *Energies*, vol. 7, no. 12, pp. 8396–8410, 2014.

[3] G. Wen, G. Hu, J. Hu, X. Shi, and G. Chen, "Frequency regulation of source-grid-load systems: A compound control strategy," *IEEE transactions on industrial informatics*, vol. 12, no. 1, pp. 69–78, 2015.

[4] D. Davies, M. Verde, O. Mnyshenko, Y. Chen, R. Rajeev, Y. Meng, and G. Elliott, "Combined economic and technological evaluation of battery energy storage for grid applications," *Nature Energy*, vol. 4, no. 1, pp. 42–50, 2019.

[5] A. Vassallo, "Applications of batteries for grid-scale energy storage," in *Advances in Batteries for Medium and Large-Scale Energy Storage*. Elsevier, 2015, pp. 587–607.

[6] S. M. Schoenung, "Energy storage systems cost update: A study for the DOE energy storage systems program." Sandia National Laboratories (SNL), Albuquerque, NM, and Livermore, CA, Tech. Rep., 2011.

[7] A. Barré, B. Deguilhem, S. Grolleau, M. Gérard, F. Suard, and D. Riu, "A review on lithium-ion battery ageing mechanisms and estimations for automotive applications," *Journal of Power Sources*, vol. 241, pp. 680–689, 2013.

[8] J. Vetter, P. Novák, M. R. Wagner, C. Veit, K.-C. Möller, J. Besenhard, M. Winter, M. Wohlfahrt-Mehrens, C. Vogler, and A. Hammouche, "Ageing mechanisms in lithium-ion batteries," *Journal of power sources*, vol. 147, no. 1-2, pp. 269–281, 2005.

[9] C. R. Birkl, M. R. Roberts, E. McTurk, P. G. Bruce, and D. A. Howey, "Degradation diagnostics for lithium ion cells," *Journal of Power Sources*, vol. 341, pp. 373–386, 2017.

[10] J. M. Reniers, G. Mulder, and D. A. Howey, "Review and performance comparison of mechanical-chemical degradation models for lithium-ion batteries," *Journal of The Electrochemical Society*, vol. 166, no. 14, p. A3189, 2019.

[11] P. Verma, P. Maire, and P. Novák, "A review of the features and analyses of the solid electrolyte interphase in li-ion batteries," *Electrochimica Acta*, vol. 55, no. 22, pp. 6332–6341, 2010.

[12] V. A. Agubra and J. W. Fergus, "The formation and stability of the solid electrolyte interface on the graphite anode," *Journal of Power Sources*, vol. 268, pp. 153–162, 2014.

[13] M. Gauthier, T. J. Carney, A. Grimaud, L. Giordano, N. Pour, H.-H. Chang, D. P. Fenning, S. F. Lux, O. Paschos, C. Bauer *et al.*, "Electrode–electrolyte interface in li-ion batteries: current understanding and new insights," *The journal of physical chemistry letters*, vol. 6, no. 22, pp. 4653–4672, 2015.

[14] K. S. N. Vikrant and S. Allu, "Modeling of lithium nucleation and plating kinetics under fast charge conditions," *Journal of The Electrochemical Society*, vol. 168, p. 020536, 2021.

[15] G. Lenze, H. Bockholt, C. Schilcher, L. Froböse, D. Jansen, U. Krewer, and A. Kwade, "Impacts of variations in manufacturing parameters on performance of lithium-ion-batteries," *Journal of The Electrochemical Society*, vol. 165, no. 2, p. A314, 2018.

[16] K. Rumpf, M. Naumann, and A. Jossen, "Experimental investigation of parametric cell-to-cell variation and correlation based on 1100 commercial lithium-ion cells," *Journal of Energy Storage*, vol. 14, pp. 224–243, 2017.

[17] B. Kenney, K. Darcovich, D. D. MacNeil, and I. J. Davidson, "Modelling the impact of variations in electrode manufacturing on lithium-ion battery modules," *Journal of Power Sources*, vol. 213, pp. 391–401, 2012.

[18] D. Shin, M. Poncino, E. Macii, and N. Chang, "A statistical model-based cell-to-cell variability management of li-ion battery pack," *IEEE Transactions on Computer-Aided Design of Integrated Circuits and Systems*, vol. 34, no. 2, pp. 252–265, 2014.

[19] K. Rumpf, A. Rheinfeld, M. Schindler, J. Keil, T. Schua, and A. Jossen, "Influence of cell-to-cell variations on the inhomogeneity of lithium-ion battery modules," *Journal of The Electrochemical Society*, vol. 165, no. 11, p. A2587, 2018.

[20] M. Dubarry, C. Pastor-Fernández, G. Baure, T. F. Yu, W. D. Widanage, and J. Marco, "Battery energy storage system modeling: Investigation of intrinsic cell-to-cell variations," *Journal of Energy Storage*, vol. 23, pp. 19–28, 2019.

[21] V. Sulzer, S. G. Marquis, R. Timms, M. Robinson, and S. J. Chapman, "Python battery mathematical modelling (pybamm)," *Journal of Open Research Software*, vol. 9, no. 1, 2021.

[22] C.-H. Chen, F. B. Planella, K. O'regan, D. Gastol, W. D. Widanage, and E. Kendrick, "Development of experimental techniques for parameterization of multi-scale lithium-ion battery models," *Journal of The Electrochemical Society*, vol. 167, no. 8, p. 080534, 2020.

[23] T. F. Fuller, M. Doyle, and J. Newman, "Simulation and optimization of the dual lithium ion insertion cell," *Journal of the Electrochemical Society*, vol. 141, no. 1, p. 1, 1994.

[24] G. Ning and B. N. Popov, "Cycle life modeling of lithium-ion batteries," *Journal of The Electrochemical Society*, vol. 151, no. 10, p. A1584, 2004.

[25] P. Ramadass, B. Haran, P. M. Gomadam, R. White, and B. N. Popov, "Development of first principles capacity fade model for li-ion cells," *Journal of the Electrochemical Society*, vol. 151, no. 2, p. A196, 2004.

[26] M. Guo, G. Sikha, and R. E. White, "Single-particle model for a lithium-ion cell: Thermal behavior," *Journal of The Electrochemical Society*, vol. 158, no. 2, p. A122, 2010.

[27] S. E. O'Kane, I. D. Campbell, M. W. Marzook, G. J. Offer, and M. Marinescu, "Physical origin of the differential voltage minimum associated with lithium plating in li-ion batteries," *Journal of The Electrochemical Society*, vol. 167, no. 9, p. 090540, 2020.

[28] S. Tippmann, D. Walper, L. Balboa, B. Spier, and W. G. Bessler, "Low-temperature charging of lithium-ion cells part I: Electrochemical modeling and experimental investigation of degradation behavior," *J. Power Sources*, vol. 252, pp. 305–316, 2014.

[29] Y. Dai, L. Cai, and R. E. White, "Simulation and analysis of stress in a li-ion battery with a blended $LiMn_2O_4$ and $LiNi_{0.8}Co_{0.15}Al_{0.05}O_2$ cathode," *Journal of power sources*, vol. 247, pp. 365–376, 2014.

[30] B. Wu and W. Lu, "A battery model that fully couples mechanics and electrochemistry at both particle and electrode levels by incorporation of particle interaction," *Journal of Power Sources*, vol. 360, pp. 360–372, 2017.

[31] J. Li, N. Lotfi, R. G. Landers, and J. Park, "A single particle model for lithium-ion batteries with electrolyte and stress-enhanced diffusion physics," *Journal of The Electrochemical Society*, vol. 164, no. 4, p. A874, 2017.

[32] J. S. Edge, S. O'Kane, R. Prosser, N. D. Kirkaldy, A. N. Patel, A. Hales, A. Ghosh, W. Ai, J. Chen, J. Yang *et al.*, "Lithium ion battery degradation: what you need to know," *Physical Chemistry Chemical Physics*, vol. 23, no. 14, pp. 8200–8221, 2021.

[33] T. G. Tranter, R. Timms, V. Sulzer, F. B. Planella, G. M. Wiggins, S. V. Karra, P. Agarwal, S. Chopra, S. Allu, P. R. Shearing, and D. J. l. Brett, "liionpack: A python package for simulating packs of batteries with pybamm," *Journal of Open Source Software*, vol. 7, no. 70, p. 4051, 2022. [Online]. Available: https://doi.org/10.21105/joss.04051

[34] S. Allu, J. J. Billings, W. R. Elwasif, S. Kalnaus, A. Kumar, D. T. Lebrun-Grandie, A. McCaskey, S. Pannala, S. Simunovic, R. W. Smith, B. R. Turcksin, and J. A. Turner, "Virtual integrated battery environment (VIBE): Version 1.2 release documentation," 12 2016. [Online]. Available: https://www.osti.gov/biblio/1474679